Appl. Phys. A 84, 231–236 (2006)
DOI: 10.1007/s00339-006-3619-8

Applied Physics A
Materials Science & Processing

Invited paper

R. ENGEL-HERBERT[1]
A. LOCATELLI[2]
S. CHERIFI[2,5]
D.M. SCHAADT[1]
J. MOHANTY[1]
K.H. PLOOG[1]
E. BAUER[2,3]
R. BELKHOU[2,4]
S. HEUN[2,6]
A. PAVLOVSKA[3]
T. LEO[7]
T. HESJEDAL[1,*,✉]

Investigation of magnetically coupled ferromagnetic stripe arrays

[1] Paul-Drude-Institut für Festkörperelektronik, Hausvogteiplatz 5–7, 10117 Berlin, Germany
[2] Sincrotrone Trieste, S.S. 14, km 163.5, 34012 Basovizza (TS), Italy
[3] Department of Physics and Astronomy, Arizona State University, P.O. Box 871504 Tempe, AZ 85287-1504, USA
[4] LURE, Bat 209D, Université Paris-Sud, BP34, 91898 Orsay, France
[5] CNRS-Laboratoire Louis Néel, BP166, 38042 Grenoble, France
[6] Laboratorio Nazionale TASC, S.S. 14, km 163.5, Area Science Park, 34012 Basovizza (TS), Italy
[7] Science and Engineering of Materials, Arizona State University, Tempe, AZ 85281, USA

Received: 28 November 2005 / Accepted: 24 April 2006
Published online: 24 May 2006 •

ABSTRACT We studied the magnetic coupling of ferromagnetic, submicron-sized stripes in the material system MnAs on GaAs. A specific coupling state, determined by stripe period and stripe width, can be tuned via film thickness and temperature, respectively. Micromagnetic imaging – in combination with micromagnetic simulations – reveals two coupling regimes. Strong magnetic coupling between the stripes creates micromagnetic domains extending across several stripes, whereas weak coupling allows for demagnetization within individual stripes. This behavior is observed for all investigated film thicknesses, since a stripe geometry leading to a given coupling scenario is a function of temperature.

PACS 68.37.Rt; 68.35.Rh; 75.70.-i; 75.70.Kw

1 Introduction

Magnetic micro- and nanostructures are of great interest for high-density data storage applications [1]. Using an individual ferromagnetic nanodot to represent a single information bit would allow the storage capacity of hard disk drives to increase by one or two orders of magnitude. Recently, the applicability of magnetic nanostructures for information processing has been discussed [2]. Especially periodic dot [3] and stripe arrays [4] are among the intensively studied candidates. The investigation of elongated magnetic nanostructures [5–7] has even been extended to one-dimensional wires [8].

In closely packed magnetic random access memory (MRAM) devices, the magnetic interaction between neighboring bits may cause the loss of stored information and thus limit the packing density of magnetic dots. In view of the important potential applications, we investigated the collective magnetic behavior of a magnetically coupled ferromagnetic wire array using micromagnetic imaging and accompanying simulations. Our model system, MnAs on GaAs(001), exhibits a self-organized array of ferromagnetic wires where the size and distance of the wires can be tuned by the film thickness and the temperature, respectively. The aim of this work is to explore the dipolar interactions – which are often undesirable – in large arrays of magnetic wires.

Different tools are available for the magnetic characterization of stripe patterns, such as MFM (magnetic force microscopy) [9], Kerr microscopy [10], PNR (polarized neutron reflectometry) [11], and XMCDPEEM (X-ray magnetic circular dichroism photo emission electron microscopy) [12]. Although the MFM technique requires no special sample preparation and allows us to perform measurements at different temperatures in applied fields [13], the deduction of the magnetization pattern from the MFM images is not straight–forward [14]. Moreover, the magnetic tip may influence the magnetization of the sample. Thus, we applied the complementary XMCDPEEM technique as it provides sufficient lateral resolution and direct access to the surface magnetization.

2 Experimental details

2.1 MnAs *on* GaAs(001)

Ferromagnetic MnAs is an uniaxial magnetic system defined by the *c*-axis of the crystal (MnAs[0001]). In bulk crystals, the magnetocrystalline easy plane of magnetization is the hexagonal basal plane [15], and the *c*-axis is the hard axis of magnetization. In epitaxial films on GaAs(001) [16, 17], the hexagon is perpendicular to the surface of GaAs. Due to shape anisotropy, thin films exhibit an easy axis of magnetization along the in-plane *a*-axis (MnAs[11$\bar{2}$0]). Furthermore, epitaxial films on GaAs(001) show a coupled, first order magneto-structural phase transition over a temperature range of 10–40 °C due to the involved strain [18]. The resulting well-ordered stripe array of ferromagnetic α-MnAs and non-ferromagnetic β-MnAs can be easily observed by atomic force microscopy as both phases have different out-of-plane lattice constants [19]. In general, wider ferromagnetic stripes in thicker films are often in a multi-domain state separated by quasi-domain walls running along the *c*-axis direction. Nar-

✉ Fax: +1 (519) 746-3077, E-mail: t.hesjedal@ece.uwaterloo.ca
**New address*: Department of Electrical and Computer Engineering, University of Waterloo, Canada

rower wires, on the other hand, tend to be single domain. The interaction between the well-ordered nanostructures is governed by magnetostatic forces.

2.2 XMCDPEEM *and* LEEM *measurements*

Following the molecular beam epitaxy growth at standard conditions [17], the samples were capped with As and transferred to the undulator beamline 'Nanospectroscopy' at ELETTRA. After the complete desorption of the As cap at approximately 320 °C in the preparation chamber at ELETTRA, low-energy electron diffraction patterns of MnAs$(\overline{1}100)(1 \times 2)$ were obtained. The XMCDPEEM and LEEM (low energy electron microscopy) measurements of the MnAs-on-GaAs(001) samples were performed with an ELMITEC microscope [20]. The samples were illuminated with the *a*-axis of MnAs (easy axis) in the plane of incidence of the light. XMCDPEEM is surface sensitive with a typical information depth of a few nanometers. Thus, for typical film thicknesses of 30–500 nm, only the magnetization distribution at the surface is imaged.

A typical LEEM image of the topography along with the magnetic XMCDPEEM image, obtained at 35 °C, is shown in Fig. 1a and b, respectively. In the topographic image, the striped phase is clearly visible. The stripes extending in height (α-phase) are ferromagnetic as can be identified by the areas of black and white contrast in the magnetic image. They are separated by non-ferromagnetic areas (grey contrast). Fig. 1c shows a close-up indicating the ferromagnetic and non-ferromagnetic areas. Its relative position is indicated in Fig. 1b by a rectangle. In the areas of black contrast in the magnetic image, the magnetization (indicated by black arrows) and the wave vector (oriented along the easy *a*-axis) are antiparallel. In white areas, magnetization (white arrows) and wave vector are parallel.

The observed domain pattern is categorized by the number of domains along the *a*-axis of a single α-stripe. Typically, up to three domains are observed termed type (I), (II) and (III), which are indicated in Fig. 1b by dashed black rectangles. A sketch of the magnetization distribution for the three domain configurations is shown in Fig. 1d. For a detailed discussion see [21].

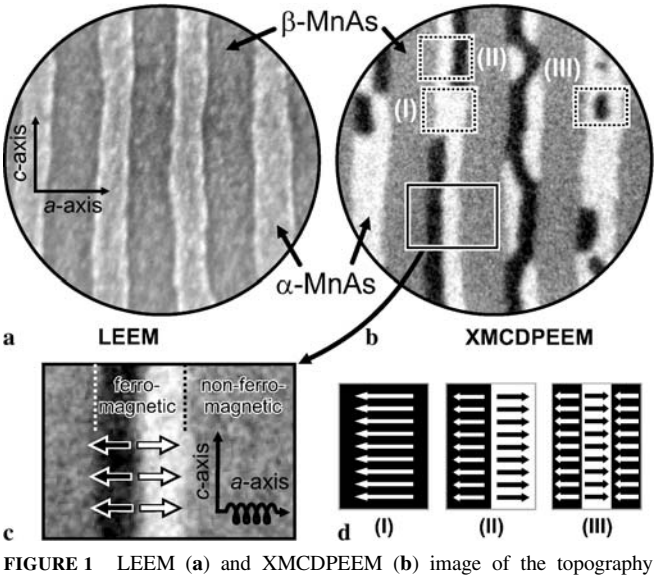

FIGURE 1 LEEM (**a**) and XMCDPEEM (**b**) image of the topography and the magnetic structure, respectively, of a 180 nm-thick MnAs film on GaAs(001). The ferromagnetic stripes are separated by non-ferromagnetic areas (grey, i.e., no magnetic contrast). The commonly observed domain types (I), (II) and (III) are indicated in (**b**) and sketched in (**d**). The magnetization direction on the ferromagnetic stripes is represented by *arrows* (**c**). It shows that the stripe magnetization is either parallel or antiparallel to the *a*-axis of the sample. Field-of-view diameter: 7 μm. Temperature $T = 35$ °C

3 Results and discussion

3.1 *Temperature–dependent* XMCDPEEM *measurements*

After the removal of the As cap layer, the samples were cooled down in the microscopy chamber to well below 0 °C. Figure 2 shows a sequence of XMCDPEEM images recorded at increasing temperatures in the same sample area (120 nm-thick film). In the complete α-phase (0 °C), the film exhibits very large single domain areas (compared to the field-of-view of 5 μm). Upon heating to the nucleation of the β-phase at 10 °C, no change in the magnetization pattern is observed. At 13 °C, the β-phase area (grey contrast) is largely unordered, and its presence has no apparent influence on the micromagnetic domain structure. At 16 °C, the β-phase tends to form a regular stripe array, and slight changes in the domain structure become apparent. At 23 °C, the β-phase is fully ordered, and a regular α–β-stripe structure is present. At this temperature, domain flipping may occur due to the separation of the extended ferromagnetic domains into smaller compartments by the introduction of β-stripes. It has to be noted that the commonly observed domain walls in the pure α-phase are inclined with respect to the easy axis. Inclined domain walls exhibit an additional stray field contribution to the total energy, compared to straight domain walls, and become unstable as soon as the large domains get separated by the introduction of β-MnAs. Domain walls running along the *a*-axis direction are favored as this eliminates the contribution of the

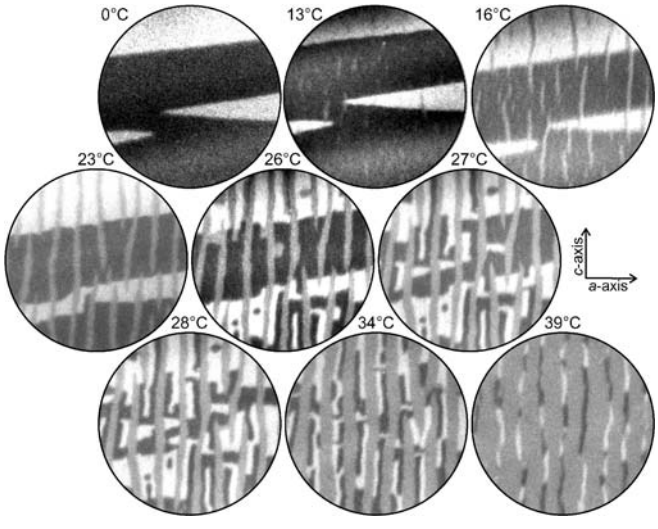

FIGURE 2 Stripe width-dependent domain patterns of a 120 nm-thick MnAs film on GaAs(001) imaged by XMCDPEEM. Field-of-view diameter: 10 μm

stray field. The inter-stripe regime is therefore characterized by extended domains across the stripes, the formation and flipping of compartments, and domain wall alignment along the a-axis direction.

The micromagnetic structure undergoes a dramatic change at 26 °C. Within the extended domains, areas of opposite magnetization nucleate. In the intra-stripe regime the demagnetization of the individual stripes is favored at larger stripe separations. If only type (I) domains are present, the demagnetization results in a rapid sequence of oppositely magnetized domains (see also Fig. 5). In the present case, however, higher order domains are also observed that are not extended across the stripes but still show an intra-stripe structure. Above 28 °C, all type (I) domains transform into type (II) domains until the stripes become so narrow that they become single domain again. Close to the phase transition at 40 °C, the α-stripes finally decompose into isolated ferromagnetic dots.

By analyzing the magnetic and structural properties of a large number of MnAs films of different thicknesses 25–500 nm), we obtained the characteristic geometrical parameters of the ferromagnetic stripes. The ferromagnetic stripe width w_α and the non-ferromagnetic stripe width w_β are a function of temperature T. Consequently, we define the α- and β-phase contents as $c_i = w_i/p$ with $i = \alpha, \beta$. The stripe period $p = w_\alpha + w_\beta$ is a linear function of the film thickness t with $p = 4.8$ t. Repeated measurements of the α-content c_α in the temperature range from 10 to 40 °C yields a linear dependency on T with a slope of $-1.6[\%]/\,°\mathrm{C}$ from 10–30 °C and a faster decay above 30 °C.

3.2 *Stripe coupling*

From the discussion of the XMCDPEEM imaging of the 120 nm-thick film, two main results can be deduced: the inter-stripe coupling, i.e., correlated domains over several α-stripes, governs the micromagnetic properties of the stripe structure up to the temperature of 26 °C. Once the inter-stripe coupling breaks down due to an increased distance between the ferromagnetic stripes, intra-stripe structures with small demagnetization fields nucleate. The formation of relatively dense antiparallel domains, or type (II) domains, leads to a reduction of the stray field energy at the cost of exchange energy.

The samples investigated with XMCDPEEM are nominally demagnetized. This is usually reached by cooling them down from the γ-phase (typically from above 300 °C) in zero applied field. However, as the field-of-view is on the micron-scale, an effective net magnetization is observed, i.e., only by averaging over larger film areas the film proves to be not magnetized. By analyzing the net magnetization and domain wall boundary length as a function of temperature (or, similarly, stripe separation), a quantitative insight into the decoupling of the stripes can be achieved. Plots of the relative areas of a ferromagnetic stripe occupied by the parallelly and antiparallelly magnetized domains are shown in Fig. 3 for four different film thicknesses: (a) 120 nm, (b) 180 nm, (c) 300 nm, and (d) 500 nm. Figure 4 shows the respective domain wall lengths between the parallelly (white) and antiparallelly (black) magnetized domains and the non-ferromagnetic areas (grey contrast). For the thinner films,

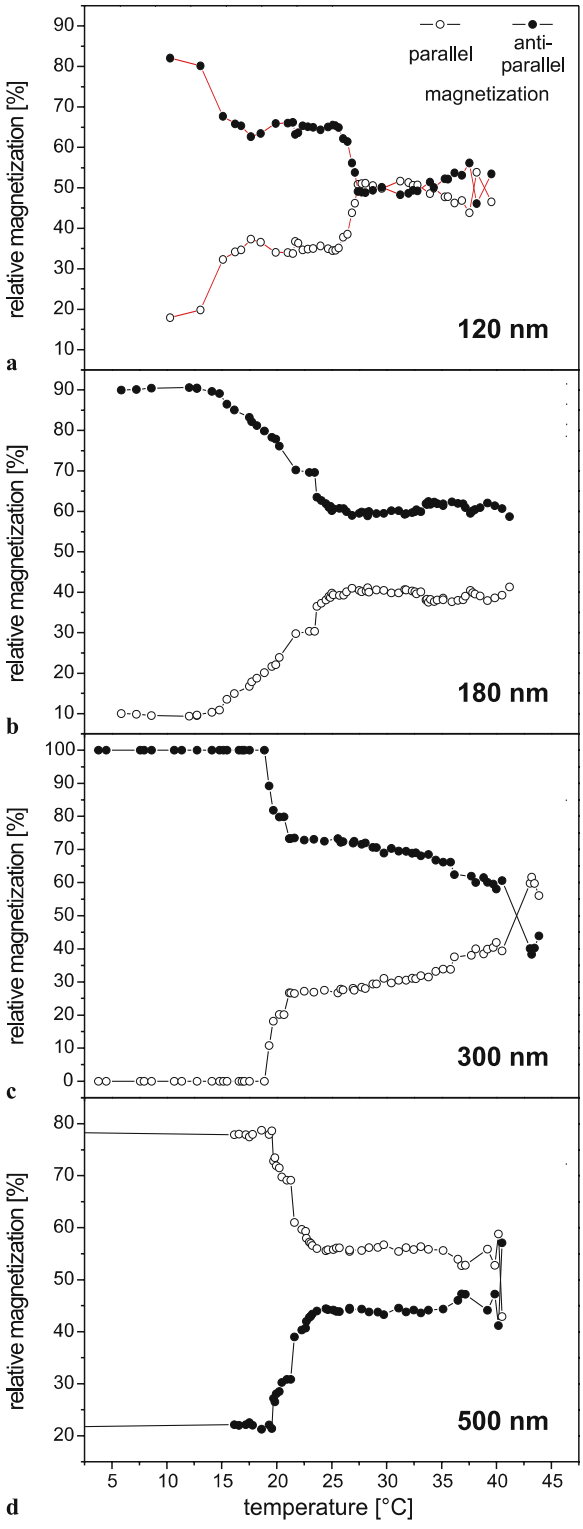

FIGURE 3 Quantitative analysis of the inter-stripe coupling behavior: plot of the parallelly and antiparallelly magnetized fraction of the ferromagnetic areas, respectively. MnAs film thickness: (**a**) 120 nm, (**b**) 180 nm, (**c**) 300 nm, and (**d**) 500 nm

a field-of-view window of 5 μm in diameter was analyzed and for the 500 nm-thick film a window of 10 μm.

Two regimes can be clearly distinguished in the plots of the relative magnetization. Let us first focus on the measurement of the 120 nm-thick film (Fig. 3a). Large relative mag-

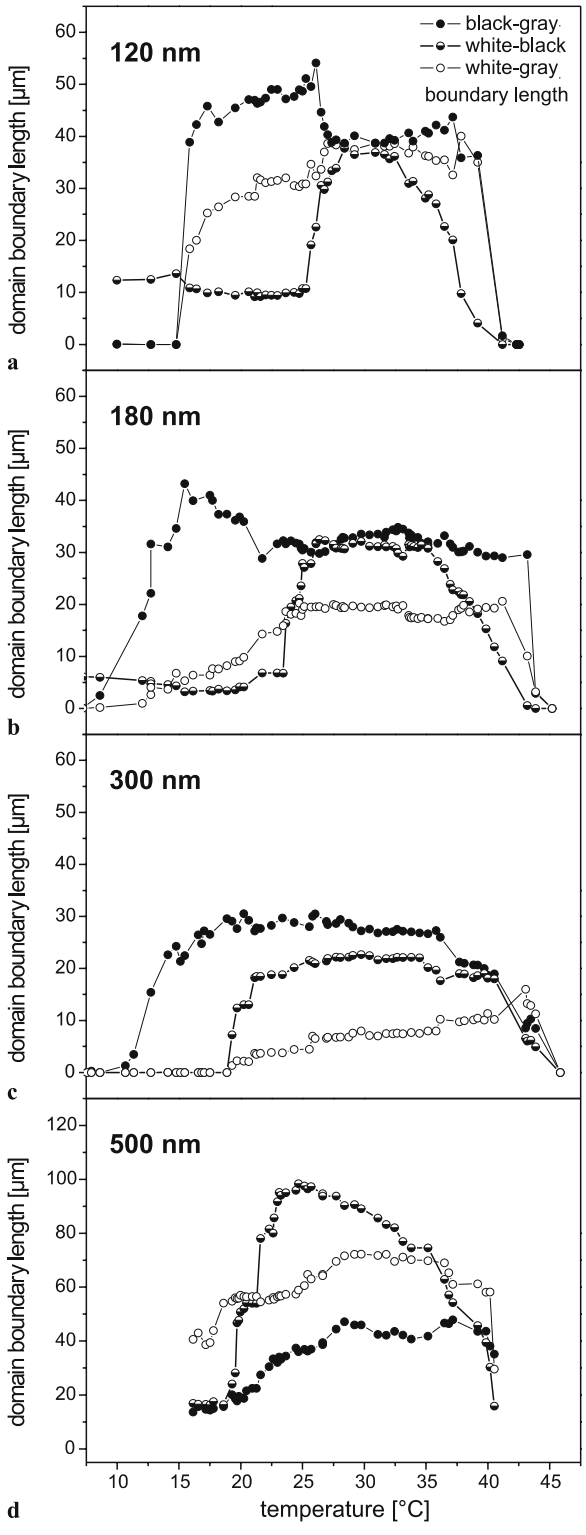

FIGURE 4 Quantitative analysis of the inter-stripe coupling behavior: length of white-gray, white-black, and black-gray boundaries, respectively. MnAs film thickness: (**a**) 120 nm, (**b**) 180 nm, (**c**) 300 nm, and (**d**) 500 nm

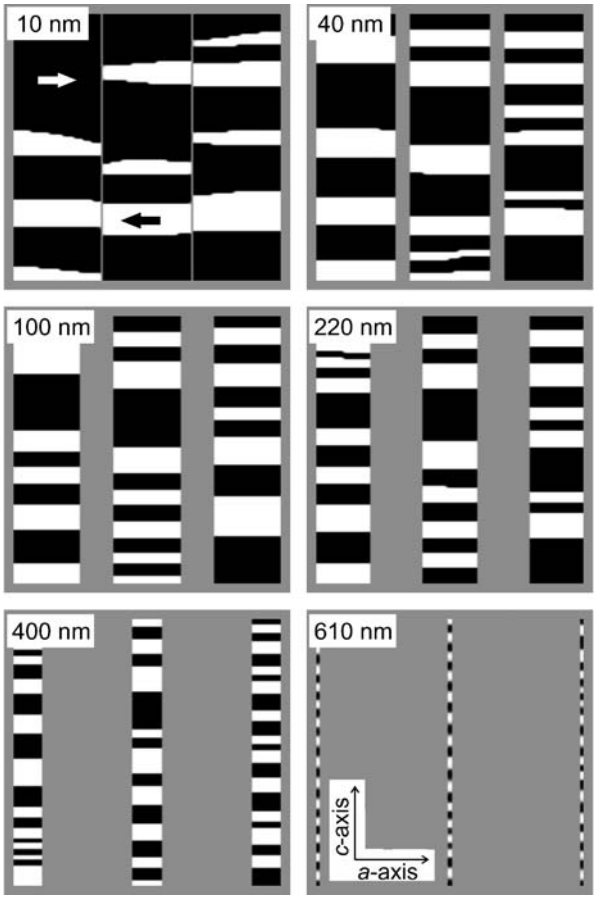

FIGURE 5 Micromagnetic simulation of the domain structure of coupled ferromagnetic stripes. The stripe separation w_β is indicated above the images. *White* and *black contrast*: parallel and antiparallel magnetizations, respectively; *grey*: non-ferromagnetic areas

netization values are found at low temperatures. A plateau with moderate smaller net magnetization is reached between 16 and 23 °C. In this plateau regime, the extended domains are more ordered across the stripes by domain flipping and domain wall movement as a result of inter-stripe coupling (cf. Fig. 2). Between 26 and 27 °C, the net magnetization vanishes as type (II) domains that show no net magnetization are introduced, replacing type (I) domains. The balancing of the different magnetization direction indicates the effective demagnetization of individual ferromagnetic stripes. This occurs most likely due to the nucleation of flux-closure domains [14], whereby the inter-stripe coupling is lost. Accompanied by the sudden drop of the ratio of parallel and antiparallel domains, a large increase in the domain boundary length between oppositely magnetized domains is found (cf. Fig. 4a).

The two coupling regimes are a universal property of the stripe array, to a certain degree independent of film thickness. Figures 3b–d and 4b–d show the plots of the net magnetization and domain wall length for three thicker samples, respectively. The ratio of the oppositely magnetized areas is different for the starting configurations. For the 180 nm-thick sample a gradual decrease of the net magnetization is observed due to a sample drift during the heating cycle. No complete demagnetization is reached up to the maximum temperature that was analyzed. In case of the 300 nm-thick film (c), the observed area is completely magnetized in one direction and the decrease of the polarization starts at $\sim$ 20 °C. Above that temperature, the relative magnetization decays very slowly in case of the 300 nm-thick film and stays roughly the same

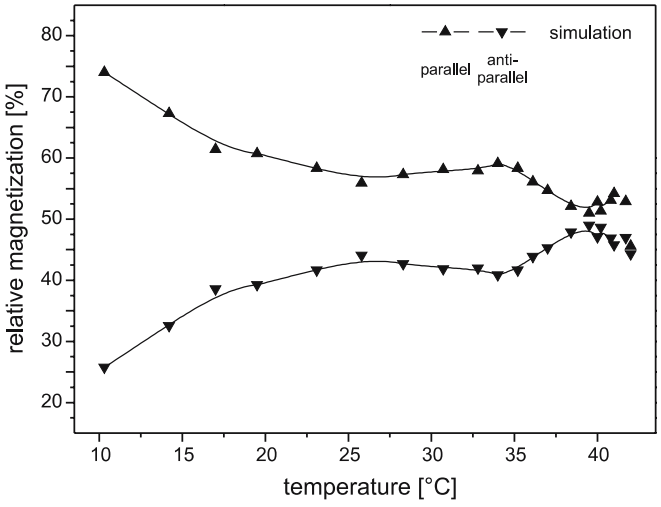

FIGURE 6 Micromagnetic simulation: Plot of the parallel and antiparallel magnetized fraction of the ferromagnetic areas of a 108 nm-thick MnAs film as a function of temperature

in case of the 500 nm-thick film. Again, no complete microscopic demagnetization was observed up to the phase transition temperature. In fact, the net magnetization after the breakdown of the inter-stripe coupling depends on the magnetization ratio at the beginning of the heating cycle and on the film thickness. This effect can be attributed to the limited field-of-view and to the formation of three-dimensional magnetization patterns in thicker films. As mentioned above, XMCDPEEM is only sensitive to the topmost layers.

All films show a steep increase in the length of the domain wall separating areas of black and white contrast at the temperature coinciding with the formation of a plateau with reduced net magnetization. This onset temperature shifts to lower values for thicker films. In general, the length of the domain wall between areas of black and white contrast is a measure of the gain of the total energy by the formation of flux-closure domains. Upon further heating, the domain wall length goes to zero as the break-up of the continuous α-stripes close to the phase transition temperature renders the stripe segments in a single domain state. Furthermore, it should be noted that the plotted domain boundary lengths in Fig. 4 are absolute values and not corrected for the amount of ferromagnetic material. In case of the 500 nm-thick film that is known to exhibit complex three-dimensional domains, a second steep increase of the domain wall length to a value of 100 μm is observed above 22 °C. As in case of the thinner films, at higher temperature and thus narrower α-stripes, the domain wall length decreases again as the single domain state is energetically preferred. It has to be noted that the tendency of thick films to form type (III) domains limits the information value of the net surface magnetization concerning the demagnetization of individual stripes. Thus, it cannot be concluded from the remaining net magnetization in case of the thicker films that the domains are not able to decouple completely.

The tendency to form enclosed domains, i.e., areas of opposite magnetization within a larger domain, can be obtained from looking at the length of the domain boundaries between ferromagnetic areas of the respective magnetization and the non-ferromagnetic areas (cf. Fig. 4, black dots and white circles). The 120 nm-thick film exhibits an equal domain boundary length for both magnetization directions with β-MnAs upon complete demagnetization (cf. Fig. 4a). On the contrary, the thicker films (180 and 300 nm) show a preference of one magnetization direction over the other in the plateau region. However, as the domain wall length between the ferromagnetic domains increases, enclosed domains form that reduce the stray field energy by their domain structure in-depth and not by the sole compensation of the surface magnetization.

3.3 *Simulations*

To obtain a deeper insight into the inter-stripe coupling due to magnetic interaction, we performed two-dimensional micromagnetic simulations. From the experiments, it can be concluded that the relevant magnetic features are domains that extend across ferromagnetic stripes (in the a-axis direction). Thus, in order to describe the coupling, the initial magnetic intra-stripe structure is not of primary importance. Since MnAs films exhibit an easy plane of magnetization perpendicular to the c-axis that plays an increasing role with decreasing contribution of the shape anisotropy for thicker films, a three-dimensional micromagnetic simulation code should, in principle, be employed. These simulations reveal the formation of an in-depth domain structure with closure domain-like features [14]. However, as three-dimensional simulations of a large array of coupling ferromagnetic stripes are very time-consuming and as closure domain-like structures do not result in a significant stray field (the magnetic interaction between stripes is strong for domains that exhibit a large stray field), less computing-intensive two-dimensional simulations are presented.

We model the α–β-phase coexistence by placing non-ferromagnetic material between three ferromagnetic stripes. The sample is 1280×1280 nm^2 (128×128 grid) and the ferromagnetic stripe width is varied from 420 nm down to 10 nm. The following parameters for MnAs were used in the two-dimensional simulation: exchange stiffness constant $A = 1.0 \times 10^{11}$ J/m, saturation magnetization $M_s = 8 \times 10^5$ A/m, and magnetocrystalline anisotropy constants $K_{u1} = -7.2 \times 10^5$ J/m^3 and $K_{u2} = 3.6 \times 10^5$ J/m^3 [14]. The y-axis of the coordinate system of the simulator corresponds to the magnetocrystalline hard axis (c-axis). The goal of the simulations is not to reproduce the micromagnetic fine structure, but to get an insight into the coupling between the stripes. Therefore, the commonly observed type (II) and (III) domains will not appear in the simulated magnetization distributions as they are in fact three-dimensional magnetization patterns [14].

As an initial configuration, the ferromagnetic α-stripes of a chosen separation w_β were assumed to be randomly magnetized. The random magnetization was allowed to relax at zero applied field. The results as a function of stripe separation are shown in Fig. 5. At a separation of $w_\beta = 10$ nm ($\hat{=}11$ °C), domains typically extend over several stripes (in the a-axis direction) and few domain walls are present, in accordance with the experimental observations. Furthermore, the domains which are not coupled across all three stripes show slightly tilted domain walls (with respect to the a-axis). As the

width of the ferromagnetic stripes is decreased, the magnetization of some areas of the stripes flips. This results in domains that extend over all three stripes, which is a fingerprint of the inter-stripe coupling. The flipping of the domains occurs predominantly for domains with previously tilted domain walls. Upon further decreasing the ferromagnetic stripe width (increasing the width of the non-ferromagnetic spacer), the spatial ordering of the domain structures vanishes as the magnetic coupling between the stripes becomes too weak. The ferromagnetic wires then try to minimize their stray fields individually, resulting in an increased number of domain walls. Upon complete decoupling of the stripes, the domain width (in the c-axis direction) becomes the same for all stripes. At a separation of $w_\beta = 610$ nm, the simulations show that the narrow stripes exhibit a predominant out-of-plane magnetization as the stripes are now narrower (20 nm) than they are thick (50 nm).

The plot of the relative magnetization is shown in Fig. 6 for a 108 nm-thick film. As in the experimental data, clearly two regimes can be distinguished. In contrast to the experiments on the 120 nm-thick film, the first decay of the net magnetization happens more gradually and is connected with the formation of extended domains across the stripes. The second decay of the net magnetization is due to the formation of compartments as the stripes are completely decoupled. Since two-dimensional simulations are not able to yield type (II) domains, the simulated demagnetization is solely due to the reduction in magnetic dipole interaction. In the future, computing-intensive three-dimensional calculations will be performed to analyze, in detail, the effects of the real magnetization distribution on the domain coupling across non-ferromagnetic stripes.

4 Conclusions

In conclusion, we investigated variations in the coupling between ferromagnetic stripes in the model system MnAs on GaAs(001). Two distinct coupling regimes were identified. First, strong inter-stripe coupling leads to micromagnetic domains extending over many stripes. With increasing stripe separation, the stripes tend to demagnetize individually. Differences between experimental observations and simulations can be attributed to more complex intra-stripe domain structures.

ACKNOWLEDGEMENTS The authors thank C. Herrmann and the Nanostructuring group for sample preparation and acknowledge support from the Bundesministerium für Bildung und Forschung (Germany). The XMCDPEEM measurements were supported by ELETTRA and the EU (HPRI-CT-1999-00033). One of us (E.B.) was additionally supported by the NSF under Grant No. 9818296 and by the ONR under Grant No. N-000140310922.

REFERENCES

1 G.A. Prinz, Science **27**, 1660 (1998)
2 P.R. Kotiuga, T. Toffoli, Physica D **120**, 139 (1998)
3 E.F. Wassermann, M. Thielen, S. Kirsch, A. Pollmann, H. Weinforth, A. Carl, J. Appl. Phys. **83**, 1753 (1998)
4 T.M. Whitney, J.S. Jiang, P.C. Searson, C.L.P. Chien, Science **261**, 1316 (1993)
5 R. Allenspach A. Bischof, Phys. Rev. Lett. **69**, 3385 (1992)
6 O. Portmann, A. Vaterlaus, D. Pescia, Nature **422**, 701 (2003)
7 J. Prokop, A. Kukunin, H.J. Elmers, Phys. Rev. Lett. **95**, 187202/1-4 (2005)
8 M. Pratzer, H.J. Elmers, M. Bode, O. Pietzsch, A. Kubetzka, R. Wiesendanger, Phys. Rev. Lett. **87**, 127201/1-4 (2001)
9 P. Eames E.D. Dahlberg, J. Appl. Phys. **91**, 7986 (2002)
10 A. Vaterlaus, U. Maier, U. Ramsperger, A. Hensch, D. Pescia, Rev. Sci. Instrum. **68**, 2800 (1997)
11 K. Theis-Bröhl, T. Schmitte, V. Leiner, H. Zabel, K. Rott, H. Brückl, J. McCord, Phys. Rev. B **67**, 184415 (2003)
12 W. Kuch, J. Gilles, S.S. Kang, S. Imada, S. Suga, J. Kirschner, Phys. Rev. B **62**, 3824 (2000)
13 J. Mohanty, R. Engel-Herbert, T. Hesjedal, Appl. Phys. A **81**, 1359 (2005)
14 R. Engel-Herbert, T. Hesjedal, J. Mohanty, D.M. Schaadt, K.H. Ploog, J. Appl. Phys. **98**, 063909 (2005)
15 R.W. De Blois, D.S. Rodbell, Phys. Rev. **130**, 1347 (1963)
16 M. Tanaka, J.P. Harbison, M.C. Park, Y.S. Park, T. Shin, G.M. Rothberg, J. Appl. Phys. **76**, 6278 (1994)
17 F. Schippan, G. Behme, L. Däweritz, K.H. Ploog, B. Dennis, K.-U. Neumann, K.R.A. Ziebeck, J. Appl. Phys. **88**, 2766 (2000)
18 V.M. Kaganer, B. Jenichen, F. Schippan, W. Braun, L. Däweritz, K.H. Ploog, Phys. Rev. B **66**, 045305 (2002)
19 T. Plake, M. Ramsteiner, V.M. Kaganer, B. Jenichen, M. Kästner, L. Däweritz, K.H. Ploog, Appl. Phys. Lett. **80**, 2523 (2002)
20 L. Däweritz, C. Herrmann, J. Mohanty, T. Hesjedal, K.H. Ploog, E. Bauer, A. Locatelli, S. Cherifi, R. Belkhou, A. Pavlovska, S. Heun, J. Vac. Sci. Technol. B **23**, 1759 (2005)
21 J.R. Mohanty, Micromagnetic investigation of MnAs thin films on GaAs surfaces (Dissertation, HU Berlin 2005), http://edoc.hu-berlin.de/dissertationen/mohanty-jyoti-ranjan-2005-06-15/PDF/Mohanty.pdf